DMD Fast Forward. Published on April 9, 2013 as doi:10.1124/dmd.113.051235

Stereoselective Glucuronidation of Ornidazole in Humans: Predominant Contribution of UDP-Glucuronosyltransferases 1A9 and 2B7

Jiangbo Du, Tiangeng You, Xiaoyan Chen, and Dafang Zhong

Shanghai Institute of Materia Medica, Chinese Academy of Sciences, Shanghai, China (J.D., X.C., D.Z.); Shanghai East Hospital, Shanghai, China (T.Y.)

DMD Fast Forward. Published on April 9, 2013 as DOI: 10.1124/dmd.113.051235
This article has not been copyedited and formatted. The final version may differ from this version.

Running Title

Glucuronidation of Ornidazole in Humans

Corresponding author: Dafang Zhong

Shanghai Institute of Materia Medica, Chinese Academy of Sciences, 501 Haike Road, Shanghai, 201203, China

Phone: +86-21-50800738; Fax: +86-21-50800738;

Email: dfzhong@mail.shcnc.ac.cn

Number of text pages: 25

Number of tables: 3

Number of figures: 6

Number of reference: 44

Number of words in the Abstract: 248

Number of words in the Introduction: 383

Number of words in the Discussion: 1491

ABBREVIATIONS: UGT, UDP-glucuronosyltransferase; HLMs, human liver microsomes; HKMs, human kidney microsomes; UPLC-Q/TOF MS, ultra-performance liquid chromatography quadrupole time-of-flight mass spectrometry; NMR, nuclear magnetic resonance; UDPGA, uridine

5'-diphosphate-glucuronic acid; BSA, bovine serum albumin; HPLC, high-performance liquid chromatography; UV, ultraviolet; CE, collision energy; MDF, mass defect filter; LC-MS/MS, liquid chromatography-tandem mass spectrometry; IS, internal standard; SD, standard deviation; AUC, plasma area under the curve; CL/F, plasma clearance; SNP, single nucleotide polymorphism.

ABSTRACT

Ornidazole [*R,S*-1-chloro-3-(2-methyl-5-nitro-1*H*-imidazol-1-yl)propan-2-ol] is a chiral 5-nitroimidazole class antimicrobial agent. This study aimed to investigate the principal metabolic pathway of ornidazole in humans and identify the major enzymes involved. A total of 19 metabolites were identified in human urine collected from patients with hepatobiliary diseases after an intravenous drip infusion of 500 mg of racemic ornidazole. Stereoselective glucuronidation, followed by renal excretion, was the principal metabolic pathway of ornidazole in humans, accounting for 37.3% of the administered dose. Screening assays with 12 available human recombinant UDP-glucuronosyltransferases (UGTs) demonstrated that UGT1A9 was the predominant UGT isoform involved in *R*-ornidazole glucuronidation, whereas *S*-ornidazole glucuronidation was almost exclusively catalyzed by UGT2B7. Chemical inhibition study with niflumic acid and flurbiprofen supported these findings. Enzyme kinetic parameters were then determined in human liver microsomes (HLMs), human kidney microsomes (HKMs), UGT1A9 and 2B7. The K_m values for UGT1A9 (15.6 ± 1.6 mM for *R*-ornidazole) and 2B7 (3.8 ± 0.9 mM for *S*-ornidazole) were quite similar to those determined in HLMs and HKMs (20.1 ± 1.4 and 17.7 ± 4.0 mM for *R*-ornidazole; 6.6 ± 1.3 and 3.2 ± 0.4 mM for *S*-ornidazole). The in vitro intrinsic clearance (CL_{int}) ratios of *S*- and *R*-ornidazole were approximately 4.3 in HLMs and 6.5 in HKMs, respectively. The hepatic and renal clearances were estimated based on the well-stirred model. Overall, stereoselective glucuronidation was the principal metabolic pathway of ornidazole in humans.

DMD Fast Forward. Published on April 9, 2013 as DOI: 10.1124/dmd.113.051235
This article has not been copyedited and formatted. The final version may differ from this version.

Furthermore, UGT1A9 and 2B7 were the predominant UGT isoforms responsible for *R*- and *S*-ornidazole glucuronidation in humans, respectively.

Introduction

Ornidazole [*R,S*-1-chloro-3-(2-methyl-5-nitro-1*H*-imidazol-1-yl)propan-2-ol] is a 5-nitroimidazole derivative used for the prophylaxis and treatment of susceptible protozoal and anaerobic bacterial infections for almost four decades (Singh et al., 2003). The antimicrobial mechanism of ornidazole involves the formation of a hydroxylamine intermediate in the microbe, which damages microbial DNA, disrupts transcription, and ultimately causes cell death (Edwards, 1979; Muller, 1983; Kedderis et al., 1989). Ornidazole, which is similar in activity to metronidazole, shows a longer half-life (14.4 h) than metronidazole (8.4 h) and has reduced dosage frequency and duration of therapy in many relevant clinical infections (Schwartz and Jeunet, 1976; Wust, 1977; Goldstein et al., 1978). Ornidazole is usually administered orally, intravenously, intravaginally, or rectally as racemates in clinical practice. Recent studies have revealed that *R*-ornidazole elicits much stronger depressant and anticonvulsant effects on the central nervous system than *S*-enantionmer (Sun et al., 2008). *S*-Ornidazole has already been developed and approved for marketing as a new antimicrobial agent in China since 2009 (http://app1.sfda.gov.cn/datasearch/face3/base.jsp).

Although ornidazole has been used for a long time, the metabolic elimination of ornidazole in humans was poorly understood. Pharmacokinetic studies have shown that ornidazole and its metabolites are predominantly excreted in urine (Schwartz and Jeunet, 1976). After an oral administration of 750 mg of ^{14}C-ornidazole (49.5 μCi), five metabolites were identified in human urine, which were the products of

hydrochloride elimination, hydrolytic dechlorination, hydroxylation, and cleavage of imidazole ring from the parent drug, respectively (Schwartz et al., 1979). However, these substances only accounted for a small fraction of the radioactivity in urine, and there was evidence of a substantial amount of conjugates and other polar metabolites in urine. In our previous study (Du et al., 2012), 12 metabolites of ornidazole in human bile were proposed based on mass fragmentation by ultra-performance liquid chromatography quadrupole time-of-flight mass spectrometry (UPLC-Q/TOF MS), but none of them were confirmed by nuclear magnetic resonance (NMR). To date, the principal metabolic pathway of ornidazole in humans is still ambiguous.

The objectives of the current study are 1) to characterize the metabolic profile of ornidazole in human urine after an intravenous drip infusion administration and identify the principal metabolic pathway of ornidazole in humans, and 2) to investigate the stereoselective glucuronidation of *S*- and *R*-ornidazole in vitro and identify the UGT isoforms mediating the glucuronidation of the two enantiomers.

Materials and Methods

Chemicals and Materials. Ornidazole and tinidazole were purchased from the National Institute for the Control of Pharmaceutical and Biological Products (Beijing, China). *S*-Ornidazole was purchased from Amresco Chemical (Solon, OH, USA). *R*-Ornidazole was synthesized and purified in our laboratory according to a previously described method with minor modifications (Hoffer and Grunberg, 1974). Uridine 5'-diphosphate-glucuronic acid (UDPGA) trisodium salt, alamethicin, bovine serum albumin (BSA), niflumic acid, and flurbiprofen were purchased from Sigma Chemical (St. Louis, MO, USA). Recombinant human UGT enzymes (UGT1A1, UGT1A3, UGT1A4, UGT1A6, UGT1A7, UGT1A8, UGT1A9, UGT1A10, UGT2B4, UGT2B7, UGT2B15, and UGT2B17) and pooled HLMs from 24 Caucasian donors (29% female, aged from 16 to 77 years) were obtained from BD Gentest (Woburn, MA, USA). Pooled HKMs from five Caucasian donors (40% female, aged from 30 to 74 years) were purchased from the Research Institute for Liver Diseases Co., Ltd. (Shanghai, China). Milli-Q water was used throughout the study and all the other solvents were of high-performance liquid chromatography (HPLC) grade or the highest grade commercially available.

Study Design, Dosing, and Sample Collection. The clinical study was approved by the ethics committee of Shanghai East Hospital (Shanghai, China), performed in compliance with the Helsinki Declaration, and consistent with the principles of Good Clinical Practice (http://www.chinafdc-law.com/laws/detail_140.html). Four patients with hepatobiliary diseases were enrolled after giving written informed consent. After

an intravenous drip infusion of 500 mg of racemic ornidazole, urine samples were collected predose (–2 to 0 h) and at 0 to 4, 4 to 8, 8 to 12, 12 to 24, 24 to 48, 48 to 72, and 72 to 96 h intervals postdose. The urine samples were stored at –20°C until analysis.

Metabolite Profiling and Characterization in Human Urine. *Sample Preparation.* Urine samples (0–24 h) were pooled by combining the volumes proportional to the total volume excreted from each subject for each collection interval. A 600-μl aliquot of acetonitrile was added to 200 μl of urine samples. The precipitate was removed via centrifugation at 14,000 ×*g* for 5 min. After evaporation to dryness, the supernatant was reconstituted in 200 μl of 10 mM ammonium acetate and methanol (90:10, v/v). A 5-μl aliquot of the reconstituted extract was injected into the UPLC-Q/TOF MS system for analysis.

UPLC-Q/TOF MS Analysis. Chromatographic separation was achieved using an Acquity UPLC system (Waters, Milford, MA, USA) on a Capcell PAK MG C18 column (4.6 × 100 mm, 5 μm; Shiseido Co., Ltd., Tokyo, Japan). The mobile phase was a mixture of 10 mM ammonium acetate (A) and methanol (B). The gradient elution started from 1% B, increased linearly to 35% B over 18 min, increased linearly to 99% B over the next 2 min, was maintained at 99% B for 2 min, and finally decreased to 1% B to re-equilibrate the column. The column temperature was set at 40°C, and the flow rate was 0.6 ml/min. The elution was monitored by UV detection at 318 nm.

MS detection was conducted utilizing a Synapt Q-TOF MS (Waters, Milford, MA,

DMD Fast Forward. Published on April 9, 2013 as DOI: 10.1124/dmd.113.051235
This article has not been copyedited and formatted. The final version may differ from this version.

USA) operated in the positive mode via an electrospray ionization interface. The capillary and cone voltages were set at 3000 and 35 V, respectively. The desolvation gas (nitrogen) was set at 800 l/h at 350°C, and the source temperature was maintained at 100°C. Data were acquired from *m/z* 50 to 1000 and corrected during acquisition using an external reference (400 ng/ml leucine enkephalin, *m/z* 556.2771) infused at 20 μl/min. The MS^E scan function was programmed with two independent collision energies (CEs). At low CE, the transfer and trap CEs were 3 and 5 eV, respectively. At high CE, the transfer CE was 10 eV and the trap CE ramped from 10 to 15 eV. The mass spectra of the urine samples were compared with blank urine using the MetaboLynx software. Mass defect filtering (MDF) function was used to screen the metabolites using a filter of 40 mDa between the filter templates and the target metabolites.

Preparation of Reference Standards of Metabolites. Pooled urine samples (0–24 h, approximately 2000 ml) were filtered with a 0.22 μm cellulose microporous membrane, and then extracted thrice with ethyl acetate. The organic layer was evaporated to dryness. The residue was dissolved in methanol–water solution (35:65, v/v) and further purified using a Shimadzu LC-6AD semipreparative HPLC apparatus equipped with an SPD-20A UV detector. Chromatographic separation was achieved on a YMC-Pack ODS-AQ column (10 × 250 mm; YMC, Inc., Wilmington, NC). The detection wavelength was set at 318 nm. Elution was performed using methanol–water–formic acid (35:65:0.065, v/v/v) at a flow rate of 3 ml/min. The eluted fractions at 8.1, 13.6, and 15.6 min were collected to obtain M6, M3, and M8,

DMD Fast Forward. Published on April 9, 2013 as DOI: 10.1124/dmd.113.051235
This article has not been copyedited and formatted. The final version may differ from this version.

respectively. After evaporation to dryness, the aqueous layer was reconstituted in methanol–water solution (10:90, v/v), and subsequently subjected to ODS-A-HG column chromatography eluted with the methanol–water (10:90, v/v) solvent system. The fractions that contained metabolites were collected and further purified in the same semipreparative HPLC system. Peaks eluted at 13.5, 17.8 and 23.0 min were collected to obtain M16-1, M10 and M16-2, respectively. M2, M4, M7 and M11 were chemically synthesized using previously described methods with modifications (Hoffer and Grunberg, 1974) except M1, which was commercially available.

The structures of the purified metabolites were characterized by UPLC-Q/TOF MS and NMR. All the NMR analysis were performed on an INOVA-400 NMR spectrometer (Varian, Inc., Palo Alto, CA). The purified metabolites were dissolved in methanol-d_4 (M3 in $CDCl_3$, M10 in DMSO-d_6, and M11 in D_2O) before analysis. Chemical shifts were provided on δ scale and referenced to tetramethylsilane at 0 ppm for ^{1}H NMR (400 MHz) and ^{13}C NMR (100 MHz).

Quantification of Ornidazole and its Metabolites in Human Urine. The concentrations of ornidazole and its metabolites were determined by UPLC with UV detection at 318 nm. The chromatographic conditions for quantification were similar to those for metabolite profiling and characterization. Calibration curves for M6, M7, M10, M16-1, M16-2, and ornidazole were linear over the following concentration ranges: 4.95 to 495 μM, 4.63 to 463 μM, 3.33 to 333 μM, 2.53 to 253 μM, 2.53 to 253 μM, and 4.57 to 457 μM, respectively. M14 and M17-1/M17-2 were semiquantified using ornidazole as calibration standard. All the calibration curves showed good

linearity with $R^2 > 0.995$.

LC-MS/MS Determination of Glucuronides. HPLC was performed using an Agilent Technologies 1200 series system that comprised a G1322A degasser, a G1312B SL binary pump, a G1357D high-performance autosampler (HiP ALS SL+) and a G1316B SL thermostated column compartment (Agilent, St. Clara, CA, USA). Ornidazole glucuronides were separated on a Capcell PAK MG C18 column (4.6 × 100 mm, 5 μm; Shiseido Co., Ltd., Tokyo, Japan) using an isocratic phase of methanol–5 mM ammonium acetate–formic acid (45:55:0.055, v/v/v) at a flow rate of 0.5 ml/min.

A 6460 triple-quadrupole mass spectrometer (Agilent, St. Clara, CA, USA) was operated with an electrospray ionization source in the positive mode. The instrument was operated at +3500 V capillary voltage and +500 V charging voltage. Nitrogen was used as a nebulizer gas at 45 psi, a carrier gas at 5 l/min at 350°C, and a sheath gas at 11 l/min at 350°C. The optimized multiple reaction monitoring fragmentation transitions were as follows: *m/z* 396 → *m/z* 220, with a fragmenter voltage of 150 V and a CE of 15 V for the two glucuronides; and *m/z* 248 → *m/z* 128, with a fragmenter voltage of 130 V and a CE of 20 V for tinidazole (internal standard, IS). The dwell time for each transition was 120 ms. The standard curves for the two glucuronides were linear from 0.5/0.5 to 500/500 ng/ml with both $R^2 > 0.995$. The accuracy and precision of the quality control samples were < 15%.

Glucuronidation in Pooled HLMs and HKMs. Preliminary experiments were performed to optimize the incubation conditions and ensure that the formation of the

DMD Fast Forward. Published on April 9, 2013 as DOI: 10.1124/dmd.113.051235
This article has not been copyedited and formatted. The final version may differ from this version.

glucuronides was within the linear range of time (15–90 min) and protein concentrations (0.25–1 mg/ml). To obtain the kinetic parameters, *R*- and *S*-ornidazole were incubated with pooled HLMs or HKMs (0.5 mg/ml) at 37°C for 60 min. All incubation mixtures contained HLMs or HKMs treated with 25 μg/ml alamethicin, 50 mM Tris-HCl buffer (pH 7.4), BSA (0% or 2%), and 8 mM $MgCl_2$ in a total volume of 200 μl. Ornidazole enantiomers were dissolved in methanol and the final concentration of methanol in the reaction mixtures was 1% (v/v). After preincubation at 37°C for 3 min, the reactions were initiated by the addition of 2 mM UDPGA, and then quenched by adding 200 μl of ice-cold acetonitrile. Incubations without UDPGA were served as negative controls. Each incubation was performed in duplicate. After spiking with 25 μl of tinidazole (1 μg/ml, IS), the mixtures were vortexed and centrifuged at 14,000 ×*g* for 5 min. The supernatant was then transferred to a glass tube and evaporated to dryness at 40°C under a stream of nitrogen. The residue was reconstituted in 100 μl of the mobile phase. A 5-μl aliquot of the reconstituted extract was injected into the LC-MS/MS system for quantification.

Glucuronidation by Recombinant UGTs. All the commercially available recombinant human UGTs (UGT1A1, 1A3, 1A4, 1A6, 1A7, 1A8, 1A9, 1A10, 2B4, 2B7, 2B15 and 2B17) were used to screen for the glucuronidation activity of racemic ornidazole at substrate concentrations of 100 μM, which is the maximal circulating therapeutic concentration of ornidazole in clinical practice, 1 mM, and 50 mM. All assays were conducted at 37°C for 60 min at a protein concentration of 0.5 mg/ml. Kinetics studies of *R*- and *S*-ornidazole by UGT1A9 and 2B7 were conducted in the

DMD Fast Forward. Published on April 9, 2013 as DOI: 10.1124/dmd.113.051235
This article has not been copyedited and formatted. The final version may differ from this version.

same condition except that the protein concentration was 0.25 mg/ml and ornidazole enantiomers were used.

Chemical Inhibition Study. Ornidazole glucuronidation in HLMs, HKMs, UGT1A9 and 2B7 were evaluated in the presence or absence of known chemical inhibitors. Niflumic acid (Miners et al., 2011) and flurbiprofen (Mano et al., 2007) were used as the corresponding inhibitors for UGT1A9 and 2B7, respectively. Racemic ornidazole (100 μM) was incubated in the absence or presence of either (0.1–50 μM) niflumic acid or flurbiprofen (5–200 μM). Incubations were performed at 37°C for 60 min in HLMs, HKMs and recombinant UGTs at the protein concentration of 0.5 mg/ml. Incubations without inhibitors were used as negative controls.

Enzyme Kinetic Data Analysis. Data were transformed and Eadie-Hofstee curves were plotted, which helped to identify the kinetic models. Kinetic parameters were then obtained by fitting the velocity data to appropriate kinetic models (Hutzler and Tracy, 2002) using GraphPad Prism 5.0 software (CA, USA).

1) Michaelis-Menten model:

$$v = \frac{V_{max} \times [S]}{K_m + [S]} \quad (1)$$

where v is the rate of metabolite formation, V_{max} is the maximum velocity, K_m is the apparent Michaelis-Menten constant (substrate concentration at half-maximal V_{max}), and [S] is the substrate concentration.

2) Substrate inhibition model:

DMD Fast Forward. Published on April 9, 2013 as DOI: 10.1124/dmd.113.051235
This article has not been copyedited and formatted. The final version may differ from this version.

$$v = \frac{V_{max}}{1 + K_m/[S] + [S]/K_{si}} \quad (2)$$

where K_{si} is the substrate inhibition constant.

The goodness of fit of data to the respective kinetic models was assessed from the R^2 values, parameter standard deviation (SD) estimates, and 95% confidence intervals. In the absence of a clear preference for a certain model, the simpler model was selected.

Protein Binding Assay. The binding of ornidazole to microsomes was estimated according to Eq. 3 (Austin et al., 2002; Liang et al., 2010):

$$f_{u,m} = \frac{1}{\left(C_{mic} \times 10^{0.56\log D - 1.41}\right) + 1} \quad (3)$$

where $f_{u,m}$ is the free fraction of ornidazole in the microsomes, C_{mic} is the microsomal protein concentration used in the incubation (0.5 mg/ml for HLMs and HKMs), and logD is the log of the octanol buffer (pH 7.4) partition coefficient (0.57 for ornidazole; calculated by ADME Suite 5.0 software, ACD/Labs).

An ultrafiltration method was developed to measure the binding of ornidazole to BSA. The filter devices for the drug binding assay were products of Millipore (Carrigtwohill, Co. Cork, Ireland), namely Amicon Ultra filters with 10 kDa Ultracel® regenerated cellulose membrane (500 µl). Three concentrations of ornidaozle (0.1, 1.0, and 10 mM) in Tris-HCl buffer (50 mM, pH 7.4) were transferred to a filter device and centrifuged at 14,000 ×*g* for 25 min. A 25-µl aliquot of the filtrate solution or the pre-filtrate solution was mixed with 75 µl of methanol and 150 µl of water, and then submitted to HPLC analysis. The experiments were performed in triplicate and the

DMD Fast Forward. Published on April 9, 2013 as DOI: 10.1124/dmd.113.051235
This article has not been copyedited and formatted. The final version may differ from this version.

nonspecific binding (*NSB*) to the filter device was calculated by Eq. 4:

$$NSB = \frac{C_{0,\mathrm{Tris}} - C_{\mathrm{u,Tris}}}{C_{0,\mathrm{Tris}}} \times 100\% \quad (4)$$

in which $C_{0,\mathrm{Tris}}$ is the substrate concentration of the pre-filtrate solutions, and $C_{\mathrm{u,Tris}}$ is the substrate concentration of the filtrate samples.

Three concentrations of ornidazole (0.1, 1.0, and 10 mM) were initially incubated with 2% BSA in Tris-HCl buffer (50 mM, pH 7.4) at 37°C for 60 min. A 500-µl aliquot of the solutions were then transferred to the filter device and centrifuged at 14,000 ×*g* for 25 min. After the filtrate fraction was removed, the filter device was placed upside down and centrifuged for 3 min at 1000 ×*g* to collect the post-filtrate fractions. A 25-µl aliquot from the filtrate fraction was mixed with 75 µl of methanol and 150 µl of water, and then submitted to HPLC analysis. A 25-µl aliquot of the pre- or post-filtrate fraction was treated with 75 µl of methanol, vortexed for 1 min, and centrifuged at 14,000 ×*g* for 5 min. The supernatant was mixed with 150 µl of water, and then subjected to HPLC analysis. Each experiment was performed in triplicate and the unbound fraction of ornidazole ($f_{\mathrm{u,BSA}}$) in 2% BSA solution was calculated by following Eq. 5:

$$f_{\mathrm{u,BSA}} = \frac{C_{\mathrm{u,BSA}}}{C_{0,\mathrm{BSA}}} \times 100\% \quad (5)$$

in which $C_{0,\mathrm{BSA}}$ is the total substrate concentration of the pre-filtrate samples, and $C_{\mathrm{u,BSA}}$ is the substrate concentration of the filtrate samples.

Prediction of Tissue Clearances. The in vivo intrinsic clearances (CL'_{int}) of ornidazole glucuronidation in the liver and the kidney were scaled up by Eq. 6 (Obach

DMD Fast Forward. Published on April 9, 2013 as DOI: 10.1124/dmd.113.051235
This article has not been copyedited and formatted. The final version may differ from this version.

et al., 1997; Liang et al., 2010; Gill et al., 2012):

$$CL'_{int} = CL_{int} \times \frac{\text{mg of microsomes}}{\text{g of tissue}} \times \frac{\text{g of tissue}}{\text{kg of weight}} \quad (6)$$

where CL_{int} is the in vitro intrinsic clearance (calculated as V_{max}/K_m). Based on the previous reports, the scaling factors for the human liver (40 mg/g and 21.4 g/kg b.wt.) and the kidney (12.8 mg/g and 4.5 g/kg b.wt.) were employed in the calculation (Al-Jahdari et al., 2006; Barter et al., 2007; Cubitt et al., 2009).

To evaluate the contribution of the liver and the kidney to the elimination of ornidazole, the hepatic clearance (CL_H) was predicted from the resulting estimated CL'_{int} using Eq. 7, based on the well-stirred model (Miners et al., 2006):

$$CL_H = \frac{Q_H \times f_{u,b} \times CL'_{int}}{Q_H + f_{u,b} \times CL'_{int}} \quad (7)$$

where $f_{u,b}$ is the unbound fraction of ornidazole in blood and Q_H is hepatic blood flow. Q_H value of 20.7 ml/min/kg b.wt. (Cubitt et al., 2009) was used. An analogous model was used for the kidney where Q_H was replaced with Q_R (average renal blood flow of 16.4 ml/min/kg b.wt.) and in vitro HKMs data were occupied (Gill et al., 2012). Unbound fractions of ornidazole in blood ($f_{u,b}$) and plasma ($f_{u,p}$) were considered equivalent for extrapolation purposes, although it is acknowledged that some difference may exist. $f_{u,p}$ was obtained from a previous report (Schwartz and Jeunet, 1976) using the equilibrium dialysis method at two concentrations (1.0 and 10 μg/ml) of ornidazole.

Results

Metabolic Profile in Human Urine. We previously reported the characterization of ornidazole metabolites in human bile by UPLC-Q/TOF MS, and the mass fragmentation pathways of ornidazole and its metabolites were proposed (Du et al., 2012). In the current study, reference standards of ornidazole metabolites were prepared and the metabolic profile of ornidazole in human urine was investigated. In human urine, a metabolic profile similar to that in human bile was found (Fig. 1). Table 1 lists the detailed information of these metabolites, including mass to charge ratio (*m*/*z*), proposed elemental composition, retention time, and the major fragment ions. The proposed metabolic pathways of ornidazole in humans are shown in Fig. 2.

A total of 19 metabolites, along with ornidazole, were detected in human urine by UPLC-Q/TOF MS. The peak at 19.5 min was assigned as the unchanged ornidazole because the retention time and mass spectral fragmentation patterns were identical to those of ornidazole. All the biliary metabolites were observed in the urine and reassigned as M3 to M17-1 based on their molecular weight and retention time (Table 1). Of note, M3, which has been proposed as a ketonic metabolite in the previous report (Du et al., 2012), was proved to be an epoxide referencing to the NMR data (Table 2). Epoxides were considered to be highly reactive intermediates that could cause severe toxicity in vivo, but M3 seemed to be deprived of reactivity for its stability in human urine and bile, although further investigation should be conducted to confirm this conjecture. Some novel metabolites were present in trace amounts in urine, including denitrated metabolite (M2), reductive dechlorinated metabolite (M4),

amino metabolite (M5), cysteine conjugate of reduced ornidazole (M12), *N*-acetylcysteine conjugate of reduced ornidazole (M15), and the diastereomer of M17-1 (M17-2). Approximately 6.0% of the administered dose was recovered as unchanged ornidazole in urine. The most abundant urinary metabolites were M16-1, followed by M6, M10, M16-2, M17, M14, and M7, which accounted for 28.9%, 11.6%, 11.4%, 8.4%, 4.8%, 2.9%, and 1.2% of the administered dose, respectively. The recovery of ornidazole and its major metabolites from urine was approximately 75.2%, in which the products of direct glucuronidation accounted for 37.3%. Based on the previous report (Du et al., 2012), the first eluted glucuronide (M16-1) was assigned as *S*-Glu, while the other (M16-2) as *R*-Glu. *S*-Glu was present at approximately 3.4 times higher than *R*-Glu in urine, indicating that the glucuronidation of ornidazole could be stereoselective in humans.

Binding of Ornidazole to Microsomes and BSA. A prerequisite for correct extrapolation of in vitro kinetic data to in vivo intrinsic clearance is being able to determine the concentration of free substrate in the incubation mixtures, or the unbound fraction (f_u). As described in *Materials and Methods*, the $f_{u,m}$ value for microsomes were predicted as 0.96 (< 5%), indicating that the binding of ornidazole to microsomes was negligible. Since lower concentration of recombinant UGTs than microsomes (0.25 versus 0.5 mg/ml) was used in the kinetics study, the binding of ornidazole to microsomes and recombinant UGTs was both ignored in the study. An ultrafiltration method was developed to evaluate the binding of ornidazole to BSA. We also took non-specific binding into consideration. The *NSB* values for different

DMD Fast Forward. Published on April 9, 2013 as DOI: 10.1124/dmd.113.051235
This article has not been copyedited and formatted. The final version may differ from this version.

concentrations were all < 2%, indicating that the non-specific binding was negligible. $f_{u,BSA}$ was 93.9%, 90.1%, and 92.3% for substrate concentrations at 0.1, 1.0, and 10 mM, respectively. Since the binding of ornidazole to microsomes and recombinant UGTs was negligible, the mean $f_{u,BSA}$ (0.92) was used to correct the apparent K_m values obtained in the incubation mixtures containing 2% BSA.

Glucuronidation in Pooled HLMs and HKMs. The "albumin effect" is observed in many drugs glucuronidated by UGT1A9 and 2B7 (Rowland et al., 2007; Rowland et al., 2008; Manevski et al., 2011). In this study, we investgated the ornidazole glucuronidation clearance in HLMs and HKMs in the presence or absence of 2% BSA (Fig. 3). *R*-Ornidazole glucuronidation in HLMs were best simulated by the Michaelis-Menten kinetic model, whereas *S*-ornidazole glucuronidation in HLMs exhibited weak substrate inhibition kinetics (K_{si} > 10 mM), as evidenced by the Eadie-Hofstee plots (Fig. 5). Glucuronidation of both enantiomers in HKMs took on Michaelis-Menten kinetic characteristics. The K_m obtained from HLMs and HKMs in the absence of BSA decreased significantly by 5.2 to 11 times when including 2% BSA in the incubation, while V_{max} values were slightly affected. The obtained kinetic parameters are listed in Table 3.

Glucuronidation in Recombinant UGTs. A panel of 12 recombinant human UGT isoforms was screened for their ornidazole glucuronidation activity at three different substrate concentrations (100 μM, 1 mM, and 50 mM). As shown in Fig. 4, at 100 μM ornidazole concentration, UGT1A9 was the only isoform that could generate detectable *R*-Glu, whereas *S*-Glu was exclusively glucuronidated by UGT2B7. No

DMD Fast Forward. Published on April 9, 2013 as DOI: 10.1124/dmd.113.051235
This article has not been copyedited and formatted. The final version may differ from this version.

other isoforms were observed to show any glucuronidation activities. At 1mM substrate concentration, UGT1A9 was still the predominant isoform mediating *R*-ornidazole glucuronidation. Relatively low activities (< 10% of UGT1A9 activity) were observed for UGT1A8 and 2B7, but not for any other isoforms. On the other hand, UGT2B7 still contributed predominantly to *S*-ornidazole glucuronidation, although few amounts of *S*-Glu could be formed by UGT1A9. At the extremely high substrate concentration of 50 mM, a panel of UGTs showed detectable *R*-ornidazole glucuronidation activities besides UGT1A9 (the highest activity), including UGT1A1, 1A3, 1A4, 1A7, 1A8, and 2B7, in which UGT2B7 and UGT1A8 accounted for approximately 45% and 33% of UGT1A9 activity, respectively. Similarly, UGT1A7, 1A8, 1A9, and 2B4 were observed to glucuronidate *S*-ornidazole besides UGT2B7 (the highest activity) at 50 mM ornidazole concentration, in which UGT1A9 accounted for about 42% of UGT2B7 activity.

Glucuronidation of ornidazole enantiomers by recombinant UGTs followed substrate inhibition kinetics (Fig. 5). As for the “albumin effect” in recombinant UGTs, a 3.2-fold decrease of the K_m obtained in the absence of BSA was observed in the case of *S*-ornidazole glucuronidation by UGT2B7, while the K_m obtained from the UGT1A9 system in the absence of BSA was only reduced by 21% when incubated with 2% BSA. The kinetic parameters are shown in Table 3.

Chemical Inhibition Study. Further information on the contribution of individual UGTs to ornidazole glucuronidation in HLMs and HKMs may be obtained from UGT inhibition experiments. Considering that UGT1A8 is mainly expressed in the

gastrointestinal tract (Ohno and Nakajin, 2009), we did not investigate the chemical inhibition of UGT1A8 in this study. Therefore, the inhibitory effects of niflumic acid and flurbiprofen on ornidazole glucuronidation were evaluated in HLMs, HKMs, UGT1A9 and 2B7. Fig. 6 shows that niflumic acid potently inhibited the formation of *R*-Glu in HLMs, HKMs, and UGT1A9 in a concentration-depend way. In the presence of niflumic acid (50 μM), *R*-ornidazole glucuronidation activities in HLMs and HKMs were reduced to 20% and 18% of the control, respectively, without any effect on the formation of *S*-Glu. Surprisingly, UGT1A9 seemed more sensitive to niflumic acid inhibition than the microsomes, especially when inhibitor concentration exceeded 1 μM (Fig. 6). On the other hand, *S*-Glu formation decreased by 78% and 86% when co-incubated with 200 μM flurbiprofen in HLMs and HKMs, respectively, while the glucuronidation of *R*-ornidazole was slightly affected. These findings strongly suggested the predominant roles of UGT1A9 and 2B7 in *R*- and *S*-ornidazole glucuronidation, respectively.

Prediction of Tissue Clearances. The CL_{int} obtained in the presence of 2% BSA (Table 3) were used to predict the contribution of the liver and the kidney to the glucuronidation clearance of ornidazole enantiomers. By scaling up, the in vivo intrinsic clearances in the liver and the kidney were estimated to be 85.1 and 4.1 μl/min/kg b.wt. for *S*-ornidazole as well as 8.0 and 0.8 μl/min/kg b.wt. for *R*-ornidazole, respectively. Based on the detected $f_{u,p}$ (0.88), the in vivo intrinsic clearance was further extrapolated to hepatic and renal clearances with the value of 74.6 and 3.6 μl/min/kg b.wt. for *S*-ornidazole as well as 7.0 and 0.7 μl/min/kg b.wt.

DMD Fast Forward. Published on April 9, 2013 as DOI: 10.1124/dmd.113.051235
This article has not been copyedited and formatted. The final version may differ from this version.

for *R*-ornidazole, respectively. Therefore, the total clearance of ornidazole via glucuronidation was estimated to be 86.0 μl/min/kg b.wt..

The average plasma clearance of ornidazole was estimated as 0.66 ml/min/kg b.wt. (ranged from 0.37 to 0.93 ml/min/kg b.wt.) from the literature reports (Lamp et al., 1999). Since approximately 50% of the recovered dose was accounted for as ornidazole glucuronides in urine, the plasma ornidazole clearance by glucuronidation in vivo may be taken as 0.33 ml/min/kg b.wt..

DMD Fast Forward. Published on April 9, 2013 as DOI: 10.1124/dmd.113.051235
This article has not been copyedited and formatted. The final version may differ from this version.

Discussion

In the present study, we investigated the metabolic profile of ornidazole in human urine after an intravenous drip infusion of 500 mg of racemic ornidazole. UPLC-Q/TOF MS analysis revealed 19 metabolites, 12 of which had been detected in human bile. Approximately 75.2% of the administered dose was recovered in urine collected up to 96 h postdose, in which glucuronidation of two ornidazole enantiomers accounted for 37.3%. These findings indicated that glucuronidation via the chiral hydroxyl was the principal metabolic pathway of ornidazole in humans. Moreover, the recovery of *S*-Glu was approximately 3.4 times higher than that of *R*-Glu, suggesting that *S*-Glu formation may be preferred compared with *R*-Glu in humans. In addition, sulfation, which accounted for 11.4% of the administered dose, is also a major metabolic pathway of ornidazole in humans. Further investigations should be conducted to determine whether or not this pathway exhibits stereoselectivity in humans.

Glucuronidation of various xenobiotics and endobiotics is catalyzed by UGTs. The UGT, a family of membrane enzymes of the endoplasmic reticulum, transfers the glucuronic acid moiety of UDPGA to substrates containing suitable functional groups, such as hydroxy, amino, or carboxy. The glucuronides formed are typically more hydrophilic than the parent chemicals, which facilitates their elimination from the body (Radominska-Pandya et al., 1999; Malik and Black, 2012). Given the increasing awareness of the importance of glucuronidation as a drug-clearance mechanism, FDA has recommended to evaluate investigational drugs as UGT substrates if

DMD Fast Forward. Published on April 9, 2013 as DOI: 10.1124/dmd.113.051235
This article has not been copyedited and formatted. The final version may differ from this version.

glucuronidation accounted for ≥ 25% of their total metabolism since 2012 (http://www.fda.gov/downloads/Drugs/GuidanceComplianceRegulatoryInformation/Guidances/UCM292362.pdf). In the current study, we investigated the stereoselective glucuronidation of ornidazole enantiomers in HLMs and HKMs, and identified the main UGT isoforms involved. For the measurement of ornidazole glucuronides, the glucuronides of ornidazole were isolated, and an LC-MS/MS method was developed.

Clinical studies have shown that the maximal plasma concentration of the therapeutic dose (1–1.5 g/d) of ornidazole was around 100 μM (Martin et al., 1990; Li et al., 2002; Wang et al., 2008; Wei et al., 2010). Therefore, the UGT isoform screening experiment was conducted at 100 μM and higher substrate concentrations (1 and 50 mM), in case of missing isoforms with low affinity. Among the 12 different UGTs evaluated, only UGT1A9 showed significant *R*-ornidazole glucuronidation activity at 100 μM ornidazole concentration, and UGT2B7 was the predominant UGT isoform responsible for the glucuronidation of *S*-ornidazole, although some other UGTs would get involved at higher substrate concentrations (Fig. 4). These findings were supported by the results of chemical inhibition study with niflumic acid and flurbiprofen. Potent inhibitory effects were observed for both inhibitors (Fig. 6). However, it should be noted that there may be some UGT-UGT interaction(s) or other UGT(s) beyond the 12 evaluated isoforms involved in *R*-ornidazole glucuronidation, as the microsomes were more resistant to niflumic acid inhibition than UGT1A9 at high inhibitor concentrations. Given UGT1A9 and 2B7 are highly expressed in the kidney (Ohno and Nakajin, 2009; Oda et al., 2012), we considered it important to

evaluate the renal clearance of ornidazole. Therefore, enzyme kinetic parameters were determined in HLMs, HKMs, UGT1A9 and 2B7. Weak substrate inhibition and classic Michaelis-Menten models were used to describe the kinetic data obtained. All the models showed satisfactory results of fitness with $R^2 \geq 0.99$. Of note, the K_m values for UGT1A9 (15.6 ± 1.6 mM) and 2B7 (3.8 ± 0.9 mM) were close to those observed in corresponding HLMs and HKMs incubations (20.1 ± 1.4 and 17.7 ± 4.0 mM for *R*-ornidazole, 6.6 ± 1.3 and 3.2 ± 0.4 mM for *S*-ornidazole), which further confirmed their predominant roles in the glucuronidation of *R*- and *S*-ornidazole, respectively. Nevertheless, there were apparent differences in kinetic model between the recombinant enzymes and the microsomes, as the recombinant enzymes tended to be more sensitive to substrate inhibition (Fig. 5). One possible reason for this is that the substantial participation of other UGTs in microsomes (e.g. UGT2B7 for *R*-ornidazole glucuronidation, UGT1A9 for *S*-ornidazole glucuronidation) at high substrate concentrations alleviated the substrate inhibition of recombinant enzymes, as evidenced by the UGT screening study at 50 mM substrate concentration (Fig. 4C).

Drug glucuronidation rates and kinetic parameters obtained from in vitro assays tend to underestimate the in vivo rates (Miners et al., 2010). Rowland et al. (Rowland et al., 2007; Rowland et al., 2008) have found that the addition of BSA significantly enhances UGT1A9 and 2B7 activities by decreasing K_m for the aglycone substrate without affecting the corresponding V_{max}. The authors also suggested that long-chain fatty acids, particularly unsaturated fatty acids, such as oleic acid, linoleic acid, and arachidonic acid, competitively inhibit the UGTs, and that BSA addition reversed that

kind of inhibition by sequestering the inhibitory fatty acids. Since similar inhibition was not observed in cultured hepatocytes (Engtrakul et al., 2005), the inhibitory fatty acids are possibly released during enzyme preparation, from either the human liver or the cells that were used for recombinant UGT expression. In the present study, the "albumin effect" of *R*- and *S*-ornidazole glucuronidation was investigated in HLMs, HKMs, UGT1A9 and 2B7. The results showed that the addition of 2% BSA increased CL_{int} by approximately 4.9- and 7.0-fold for *R*-ornidazole in HLMs and HKMs, respectively. Approximately 12- and 5.8-fold increase of CL_{int} for *S*-ornidazole in HLMs and HKMs were observed, respectively. The pictures in recombinant UGTs were less dramatic than those in HLMs and HKMs, with approximately 1.3- and 2.9-fold increase of CL_{int} for UGT1A9 and 2B7, respectively. A possible reason for this is the relatively low fatty acid content in the recombinant UGTs expression system.

Ornidazole glucuronidation exhibited stereoslecetivity in HLMs and HKMs. The ratios of CL_{int} for *S*-Glu and *R*-Glu formation were approximately 4.3 in HLMs and 6.5 in HKMs, indicating a preference for *S*-ornidazole glucuronidation. For the paucity of relevant pharmacokinetics reports, the ratio of *R*-Glu to *S*-Glu in human plasma (or blood) was not available. Nevertheless, we could still get a clue from the ratio of ornidazole enantiomers in the circulation. After an oral administration of 1000 mg racemic ornidazole to an healthy male volunteer, the plasma levels of *S*-ornidazole were lower than those of *R*-ornidazole in the elimination phase, with the plasma area under the curve (AUC) ratio of *S*-ornidazole to *R*-ornidazole being about 0.76 and

DMD Fast Forward. Published on April 9, 2013 as DOI: 10.1124/dmd.113.051235
This article has not been copyedited and formatted. The final version may differ from this version.

plasma clearance (CL/F) values ratio around 1.3 (Wang et al., 2008). As glucuronidation followed by renal excretion was the primary elimination way of ornidazole, the different glucuronidation clearances of *S*- and *R*-ornidazole would certainly play an important role in the stereoselective pharmacokinetics of ornidazole enantiomers in humans. N^+-glucuronidation of morinidazole, another 5-nitroimidzaole class antimicrobial agent which is currently in Phase III clinical trials in China, is stereoselective in humans (Gao et al., 2012). The different rate of glucuronidation by UGT1A9 is the major determinant of the stereoselectivity.

Extrapolation of the kinetic constants (e.g., CL_{int}) generated in the presence of BSA have been reported to improve the prediction of in vivo clearances for many drugs (Rowland et al., 2008). Therefore, the CL_{int} obtained in the presence of 2% BSA were used to predict the hepatic and renal clearances of ornidazole glucuronidation. Since there are no kidney-specific models available for in vitro-in vivo extrapolation study, the well-stirred model was applied herein for the kidney, although it may cause some biases (Gill et al., 2012). Prediction results showed that the glucuronidation clearances of both enantiomers in the liver were much larger than those in the kidney (74.6 versus 3.6 µl/min/kg b.wt. for *S*-ornidazole; 7.0 versus 0.7 µl/min/kg b.wt. for *R*-ornidazole), which suggested that the liver might play the major role in ornidazole metabolic clearance via glucuronidation. Notably, the scaled-up total clearance (~0.1 ml/min/kg b.wt.) correctly predicted the magnitude of the reported mean in vivo clearance (~0.33 ml/min/kg b.wt.). Nevertheless, the well-stirred model still underpredicted the in vivo clearance by approximately 3.8-fold, which may be due to

the involvement of other mechanisms (e.g. transporters) in vivo or the systematic error of this algorithm (Ito et al., 1998; Uchaipichat et al., 2006).

Genetic polymorphisms have been reported in quite a few UGT family members (Argikar et al., 2008; Court, 2010). Several single nucleotide polymorphisms (SNPs) of UGT1A9 (UGT1A9*2, UGT1A9*3, and UGT1A9*5) and UGT2B7 (UGT2B7*71S, UGT2B7*2, and UGT2B7*5) have been described in the literature, and a range of catalytic activity change are observed towards different substrates (Villeneuve et al., 2003; Takahashi et al., 2008; Wang et al., 2011). Given that the glucuronidation of ornidazole enantiomers was almost exclusively manipulated by UGT1A9 and 2B7, it is reasonable to speculate that fluctuating concentrations of *S*- and *R*-ornidazole due to the UGT1A9 and/or 2B7 polymorphisms could be encountered in the clinical use of racemic ornidazole, which would be potentially of toxicological and therapeutic importance.

In conclusion, 1) glucuronidation of the chiral hydroxyl was the principal metabolic pathway of ornidazole in humans; 2) this pathway exhibited stereoselectivity in humans: *S*-ornidazole showed a higher glucuronidation rate than *R*-enantiomer; and 3) recombinant UGT screening, chemical inhibition, and kinetic studies clearly indicated that UGT1A9 and 2B7 were the predominant UGTs responsible for *R*- and *S*-ornidazole glucuronidation, respectively.

DMD Fast Forward. Published on April 9, 2013 as DOI: 10.1124/dmd.113.051235
This article has not been copyedited and formatted. The final version may differ from this version.

Acknowledgements

We would like to express our gratitude to Dr. Lei Wang for the kind assistance in NMR analysis and Dr. Liping Ma for sharing her expertise in enzyme kinetics experiments.

DMD Fast Forward. Published on April 9, 2013 as DOI: 10.1124/dmd.113.051235
This article has not been copyedited and formatted. The final version may differ from this version.

Authorship Contributions

Participated in research design: Du, You, Chen, and Zhong.

Conducted experiments: Du and You.

Contributed new reagents or analytic tools: Du, You, Chen, and Zhong.

Preformed data analysis: Du, Chen, and Zhong.

Contributed to the writing of the manuscript: Du and Zhong.

References

Al-Jahdari WS, Yamamoto K, Hiraoka H, Nakamura K, Goto F, and Horiuchi R (2006) Prediction of total propofol clearance based on enzyme activities in microsomes from human kidney and liver. *Eur J Clin Pharmacol* **62:**527-533.

Argikar UA, Iwuchukwu OF, and Nagar S (2008) Update on tools for evaluation of uridine diphosphoglucuronosyltransferase polymorphisms. *Expert Opin Drug Metab Toxicol* **4:**879-894.

Austin RP, Barton P, Cockroft SL, Wenlock MC, and Riley RJ (2002) The influence of nonspecific microsomal binding on apparent intrinsic clearance, and its prediction from physicochemical properties. *Drug Metab Dispos* **30:**1497-1503.

Barter ZE, Bayliss MK, Beaune PH, Boobis AR, Carlile DJ, Edwards RJ, Houston JB, Lake BG, Lipscomb JC, Pelkonen OR, Tucker GT, and Rostami-Hodjegan A (2007) Scaling factors for the extrapolation of in vivo metabolic drug clearance from in vitro data: reaching a consensus on values of human microsomal protein and hepatocellularity per gram of liver. *Curr Drug Metab* **8:**33-45.

Court MH (2010) Interindividual variability in hepatic drug glucuronidation: studies into the role of age, sex, enzyme inducers, and genetic polymorphism using the human liver bank as a model system. *Drug Metab Rev* **42:**209-224.

Cubitt HE, Houston JB, and Galetin A (2009) Relative importance of intestinal and hepatic glucuronidation-impact on the prediction of drug clearance. *Pharm*

Res **26:**1073-1083.

Du JB, Deng P, Chen XY, Wang HD, You TG, and Zhong DF (2012) Characterization of ornidazole metabolites in human bile after intraveneous doses by ultraperformance liquid chromatography/quadrupole time-of-flight mass spectrometry. *Acta Pharm Sin B* **2:**159-167.

Edwards DI (1979) Mechanism of antimicrobial action of metronidazole. *J Antimicrob Chemother* **5:**499-502.

Engtrakul JJ, Foti RS, Strelevitz TJ, and Fisher MB (2005) Altered AZT (3'-azido-3'-deoxythymidine) glucuronidation kinetics in liver microsomes as an explanation for underprediction of in vivo clearance: comparison to hepatocytes and effect of incubation environment. *Drug Metab Dispos* **33:**1621-1627.

Gao RN, Li L, Xie C, Diao XX, Zhong DF, and Chen XY (2012) Metabolism and pharmacokinetics of morinidazole in humans: identification of diastereoisomeric morpholine N+-glucuronides catalyzed by UDP glucuronosyltransferase 1A9. *Drug Metab Dispos* **40:**556-567.

Gill KL, Houston JB, and Galetin A (2012) Characterization of in vitro glucuronidation clearance of a range of drugs in human kidney microsomes: comparison with liver and intestinal glucuronidation and impact of albumin. *Drug Metab Dispos* **40:**825-835.

Goldstein EJ, Sutter VL, and Finegold SM (1978) Comparative susceptibilities of anaerobic bacteria to metronidazole, ornidazole, and SC-28538. *Antimicrob*

Agents Chemother **14:**609-613.

Hoffer M and Grunberg E (1974) Synthesis and antiprotozoal activity of 1-(3-chloro-2-hydroxypropyl)-substituted nitroimidazoles. *J Med Chem* **17:**1019-1020.

Hutzler JM and Tracy TS (2002) Atypical kinetic profiles in drug metabolism reactions. *Drug Metab Dispos* **30:**355-362.

Ito K, Iwatsubo T, Kanamitsu S, Nakajima Y, and Sugiyama Y (1998) Quantitative prediction of in vivo drug clearance and drug interactions from in vitro data on metabolism, together with binding and transport. *Annu Rev Pharmacol Toxicol* **38:**461-499.

Kedderis GL, Argenbright LS, and Miwa GT (1989) Covalent interaction of 5-nitroimidazoles with DNA and protein in vitro: mechanism of reductive activation. *Chem Res Toxicol* **2:**146-149.

Lamp KC, Freeman CD, Klutman NE, and Lacy MK (1999) Pharmacokinetics and pharmacodynamics of the nitroimidazole antimicrobials. *Clin Pharmacokinet* **36:**353-373.

Li Q, Wang BJ, and Guo RC (2002) Study of the pharmacokinetics and bioequlvalance of ornidazole capsules and imported ornidazole tablets in healthy volunteers. *Chin J Clin PharmacoI* **18:**119-121.

Liang SC, Ge GB, Liu HX, Zhang YY, Wang LM, Zhang JW, Yin L, Li W, Fang ZZ, Wu JJ, Li GH, and Yang L (2010) Identification and characterization of human UDP-glucuronosyltransferases responsible for the in vitro glucuronidation of

daphnetin. *Drug Metab Dispos* **38:**973-980.

Malik V and Black GW (2012) Structural, functional, and mutagenesis studies of UDP-glycosyltransferases. *Adv Protein Chem Struct Biol* **87:**87-115.

Manevski N, Moreolo PS, Yli-Kauhaluoma J, and Finel M (2011) Bovine serum albumin decreases Km values of human UDP-glucuronosyltransferases 1A9 and 2B7 and increases Vmax values of UGT1A9. *Drug Metab Dispos* **39:**2117-2129.

Mano Y, Usui T, and Kamimura H (2007) Predominant contribution of UDP-glucuronosyltransferase 2B7 in the glucuronidation of racemic flurbiprofen in the human liver. *Drug Metab Dispos* **35:**1182-1187.

Martin C, Bruguerolle B, Mallet MN, Condomines M, Sastre B, and Gouin F (1990) Pharmacokinetics and tissue penetration of a single dose of ornidazole (1,000 milligrams intravenously) for antibiotic prophylaxis in colorectal surgery. *Antimicrob Agents Chemother* **34:**1921-1924.

Miners JO, Bowalgaha K, Elliot DJ, Baranczewski P, and Knights KM (2011) Characterization of niflumic acid as a selective inhibitor of human liver microsomal UDP-glucuronosyltransferase 1A9: application to the reaction phenotyping of acetaminophen glucuronidation. *Drug Metab Dispos* **39:**644-652.

Miners JO, Knights KM, Houston JB, and Mackenzie PI (2006) In vitro-in vivo correlation for drugs and other compounds eliminated by glucuronidation in humans: pitfalls and promises. *Biochem Pharmacol* **71:**1531-1539.

Miners JO, Mackenzie PI, and Knights KM (2010) The prediction of drug-glucuronidation parameters in humans: UDP-glucuronosyltransferase enzyme-selective substrate and inhibitor probes for reaction phenotyping and in vitro-in vivo extrapolation of drug clearance and drug-drug interaction potential. *Drug Metab Rev* **42:**196-208.

Muller M (1983) Mode of action of metronidazole on anaerobic bacteria and protozoa. *Surgery* **93:**165-171.

Obach RS, Baxter JG, Liston TE, Silber BM, Jones BC, MacIntyre F, Rance DJ, and Wastall P (1997) The prediction of human pharmacokinetic parameters from preclinical and in vitro metabolism data. *J Pharmacol Exp Ther* **283:**46-58.

Oda S, Nakajima M, Hatakeyama M, Fukami T, and Yokoi T (2012) Preparation of a Specific Monoclonal Antibody against Human UDP-Glucuronosyltransferase (UGT) 1A9 and Evaluation of UGT1A9 Protein Levels in Human Tissues. *Drug Metab Dispos* **40:**1620-1627.

Ohno S and Nakajin S (2009) Determination of mRNA expression of human UDP-glucuronosyltransferases and application for localization in various human tissues by real-time reverse transcriptase-polymerase chain reaction. *Drug Metab Dispos* **37:**32-40.

Radominska-Pandya A, Czernik PJ, Little JM, Battaglia E, and Mackenzie PI (1999) Structural and functional studies of UDP-glucuronosyltransferases. *Drug Metab Rev* **31:**817-899.

Rowland A, Gaganis P, Elliot DJ, Mackenzie PI, Knights KM, and Miners JO (2007)

Binding of inhibitory fatty acids is responsible for the enhancement of UDP-glucuronosyltransferase 2B7 activity by albumin: implications for in vitro-in vivo extrapolation. *J Pharmacol Exp Ther* **321:**137-147.

Rowland A, Knights KM, Mackenzie PI, and Miners JO (2008) The "albumin effect" and drug glucuronidation: bovine serum albumin and fatty acid-free human serum albumin enhance the glucuronidation of UDP-glucuronosyltransferase (UGT) 1A9 substrates but not UGT1A1 and UGT1A6 activities. *Drug Metab Dispos* **36:**1056-1062.

Schwartz DE and Jeunet F (1976) Comparative pharmacokinetic studies of ornidazole and metronidazole in man. *Chemotherapy* **22:**19-29.

Schwartz DE, Jordan JC, Vetter W, and Oesterhelt G (1979) Metabolic studies of ornidazole in the rat, in the dog and in man. *Xenobiotica* **9:**571-581.

Singh P, Mittal R, Sharma GC, Singh S, and Singh A (2003) Ornidazole: comprehensive profile. *Profiles Drug Subst Excip Relat Methodol* **30:**123-184.

Sun JH, Wang ZQ, Gu XL, and Mu R (2008) Comparative study of ornidazole enantiomers on the toxic and side effects to central nervous system in mice. *J China Pharm Univ* **39:**343-347.

Takahashi H, Maruo Y, Mori A, Iwai M, Sato H, and Takeuchi Y (2008) Effect of D256N and Y483D on propofol glucuronidation by human uridine 5'-diphosphate glucuronosyltransferase (UGT1A9). *Basic Clin Pharmacol Toxicol* **103:**131-136.

Uchaipichat V, Winner LK, Mackenzie PI, Elliot DJ, Williams JA, and Miners JO

(2006) Quantitative prediction of in vivo inhibitory interactions involving glucuronidated drugs from in vitro data: the effect of fluconazole on zidovudine glucuronidation. *Br J Clin Pharmacol* **61:**427-439.

Villeneuve L, Girard H, Fortier LC, Gagne JF, and Guillemette C (2003) Novel functional polymorphisms in the UGT1A7 and UGT1A9 glucuronidating enzymes in Caucasian and African-American subjects and their impact on the metabolism of 7-ethyl-10-hydroxycamptothecin and flavopiridol anticancer drugs. *J Pharmacol Exp Ther* **307:**117-128.

Wang H, Chen Y, Zhou J, Ma C, Chen YC, and Liu XQ (2008) Stereoselective determination of ornidazole enantiomers in human plasma and urine samples by chiral LC: Application to pharmacokinetic study. *Chromatographia* **67:**875-881.

Wang HN, Yuan LM, and Zeng S (2011) Characterizing the effect of UDP-glucuronosyltransferase (UGT) 2B7 and UGT1A9 genetic polymorphisms on enantioselective glucuronidation of flurbiprofen. *Biochem Pharmacol* **82:**1757-1763.

Wei MJ, Li TY, Zhao CY, Zhang P, Kang ZS, Liu Y, and Lv Y (2010) Bioequivalence of ornidazole tablets in Chinese healthy volunteers. *Chin J Clin PharmacoI* **26:**822-825.

Wust J (1977) Susceptibility of anaerobic bacteria to metronidazole, ornidazole, and tinidazole and routine susceptibility testing by standardized methods. *Antimicrob Agents Chemother* **11:**631-637.

DMD Fast Forward. Published on April 9, 2013 as DOI: 10.1124/dmd.113.051235
This article has not been copyedited and formatted. The final version may differ from this version.

Figure Legends

Fig. 1. Metabolic profile in pooled human urine 0–24 h after an intravenous drip infusion of 500 mg of racemic ornidazole. (A) MDF metabolic profile and (B) UPLC-UV chromatogram. AU, arbitrary unit.

Fig. 2. Proposed metabolic pathway of ornidazole in humans.

Fig. 3. The typical chromatograms of ornidazole glucuronides (A, B) and IS (C). Segment 1, to waste; segment 2, to source; segment 3, to waste.

Fig. 4. Glucuronidation of racemic ornidazole at concentrations of 100 μM (A), 1 mM (B), and 50 mM (C) by 12 human recombinant UGTs. Each column represents the mean of duplicate determinations.

Fig. 5. Kinetic profiles of *R*- and *S*-ornidazole glucuronidation in the absence of 2% BSA by HLMs (A, D), HKMs (B, E), UGT1A9 (C) and UGT2B7(F), as well as in the presence of 2% BSA by HLMs (a, d), HKMs (b, e), UGT1A9 (c) and UGT2B7 (f). Eadie-Hofstee plots (*V/S* versus *V*) are displayed as insets. Data points represent the mean of duplicate determinations.

Fig. 6. Effects of chemical inhibitors (A, Niflumic acid; B, Flurbiprofen) on the glucuronidation of racemic ornidazole in HLMs, HKMs, UGT1A9 and 2B7. The control activities for *S*-Glu and *R*-Glu formation in the respective UGT sources in the absence of inhibitors were normalized to 100%. Each column represents the mean of duplicate determinations.

DMD Fast Forward. Published on April 9, 2013 as DOI: 10.1124/dmd.113.051235
This article has not been copyedited and formatted. The final version may differ from this version.

Table 1. Identification of ornidazole metabolites in humans after an intravenous drip infusion of 500 mg of racemic ornidazole using UPLC-Q/TOF MS. The bile data were obtained from the previous report (Du et al., 2012).

Metabolite	Description	*m/z* [M+H]+	Formula	Retention time min	Excretion pathway	Major fragment ions
M0	Parent	220.049	$C_7H_{10}ClN_3O_3$	19.5	urine, bile	128.043, 82.050
M1	*N*-Dealkylation	128.046	$C_4H_5N_3O_2$	7.2	urine	82.052
M2	Denitration	175.064	$C_7H_{11}ClN_2O$	8.6	urine	83.059
M3	HCl elimination	184.072	$C_7H_9N_3O_3$	16.3	urine, bile	128.046, 82.053
M4	Reductive dechlorination	186.088	$C_7H_{11}N_3O_3$	16.5	urine	128.046, 82.053
M5	Reduction of nitro	190.075	$C_7H_{12}ClN_3O$	7.0	urine	120.021, 98.071
M6	Hydration of M3	202.082	$C_7H_{11}N_3O_4$	11.0	urine, bile	128.043, 82.051
M7	ω-Carboxylation of M6	216.062	$C_7H_9N_3O_5$	5.9	urine, bile	128.044, 82.052
M8	Hydroxylation	236.043	$C_7H_{10}ClN_3O_4$	15.2	urine, bile	144.037, 126.027
M9	Cysteine conjugation – NO_2	294.067	$C_{10}H_{16}ClN_3O_3S$	11.9	urine, bile	248.063/250.059, 207.034/ 209.032, 115.032
M10	Sulfation	300.005	$C_7H_{10}ClN_3O_6S$	16.2	urine, bile	220.049/222.048, 128.044, 82.052
M11	Cysteine conjugation – Cl	305.092	$C_{10}H_{16}N_4O_5S$	9.6	urine, bile	178.052, 128.045, 88.038
M12	Cysteine conjugation of reduced ornidazole	309.077	$C_{10}H_{17}ClN_4O_3S$	10.2	urine	222.055/224.032, 292.055/294.048, 188.059/190.041, 130.043
M13	*N*-Acetylcysteine conjugation – NO_2	336.078	$C_{12}H_{18}ClN_3O_4S$	13.5	urine, bile	294.067, 207.034/209.032, 115.034
M14	*N*-Acetylcysteine conjugation – Cl	347.103	$C_{12}H_{18}N_4O_6S$	13.7	urine, bile	178.048, 130.049, 84.044, 82.054
M15	*N*-Acetylcysteine conjugation of reduced ornidazole	351.086	$C_{12}H_{19}ClN_4O_4S$	11.4	urine	309.072/311.071, 222.044/224.041, 130.043
M16-1	Glucuronization of *S*-ornidazole	396.080	$C_{13}H_{18}ClN_3O_9$	13.1	urine, bile	220.049/222.047, 128.043
M16-2	Glucuronization of *R*-ornidazole	396.080	$C_{13}H_{18}ClN_3O_9$	14.6	urine, bile	220.049/222.045, 128.043
M17-1	Glucuronization of M8	412.075	$C_{13}H_{18}ClN_3O_{10}$	9.3	urine, bile	236.044/238.040, 144.040, 126.029
M17-2	Glucuronization of M8	412.075	$C_{13}H_{18}ClN_3O_{10}$	9.5	urine	236.044/238.043, 144.039, 126.029

Table 2. ^{1}H and ^{13}C NMR data as well as chemical shift assignments for ornidazole and its metabolites.

Position *	Ornidazole		M1		M2		M3		M4		M6	
	$\delta^{1}H$ (*J* /Hz)	$\delta^{13}C$	$\delta^{1}H$ (*J* /Hz)	$\delta^{13}C$	$\delta^{1}H$ (*J* /Hz)	$\delta^{13}C$	$\delta^{1}H$ (*J* /Hz)	$\delta^{13}C$	$\delta^{1}H$ (*J* /Hz)	$\delta^{13}C$	$\delta^{1}H$ (*J* /Hz)	$\delta^{13}C$
2		154.3		149.1		147.6		151.8		153.9		154.1
4	7.94 (1H, s)	133.3	7.94 (1H, s)	119.7	7.02 (1H, d, 1.4)	128.0	7.96 (1H, s)	133.2	7.92 (1H, s)	133.3	7.93 (1H, s)	133.3
5		141.0		147.5	6.80 (1H, s, 1.4)	122.4		138.7		140.9		141.0
6	2.52 (3H, s)	15.3	2.39 (3H, s)	14.5	2.37 (3H, s)	14.7	2.50 (3H, s)	14.7	2.51 (3H, s)	15.3	2.52 (3H, s)	15.3
1'	4.69 (1H, dd, 14.2, 2.7)	48.3			4.13 (1H, dd, 13.4, 2.8)	47.9	4.88 (1H, dd, 15.0, 2.2)	45.4	4.88 (1H, dd, 13.9, 2.5)	55.0	4.62 (1H, dd, 14.3, 3.0)	51.3
	4.26 (1H, dd, 14.2, 7.9)				3.96 (1H, dd, 13.4, 7.5)		4.19 (1H, dd, 15.0, 5.9)		4.11 (1H, dd, 13.9, 9.2)		4.22 (1H, dd, 14.3, 9.4)	
2'	4.11 (1H, m)	72.0			4.00–4.05 (1H, m)	72.7	3.34–3.41 (1H, m)	50.7	3.97–4.06 (1H, m)	68.6	3.91 (1H, m)	73.0
3'	3.55–3.77 (2H, m)	51.6			3.47–3.60 (2H, m)	50.8	2.88 (1H, t, 4.2)	47.9	1.25 (3H, s)	21.8	3.54–3.66 (2H, m)	65.9
							2.52 (1H, dd, 4.2, 2.5)					

* Positional assignments are shown in Fig. 2.

s, singlet; d, doublet; t, triplet; m, multiplet.

Table 2. (*continued*)

Position *	M7		M8		M10		M11		M16-1		M16-2	
	δ^1H (*J* /Hz)	δ^{13}C	δ^1H (*J* /Hz)	δ^{13}C	δ^1H (*J* /Hz)	δ^{13}C	δ^1H (*J* /Hz)	δ^{13}C	δ^1H (*J* /Hz)	δ^{13}C	δ^1H (*J* /Hz)	δ^{13}C
2		154.0		155.0		154.4		154.1		154.1		154.7
4	7.89 (1H, s)	133.1	7.97 (1H, s)	133.3	7.97 (1H, s)	133.4	8.01 (1H, s)	133.7	7.82 (1H, s)	133.7	7.96 (1H, s)	133.2
5		141.2		141.5		141.0		141.0		141.0		140.8
6	2.52 (3H, s)	15.3	4.83 (1H, d, 13.7) 4.69 (1H, d, 13.7)	48.3	2.41 (3H, s)	15.2	2.45 (3H, s)	18.1	2.49 (3H, s)	15.3	2.56 (3H, s)	15.4
1'	4.82 (1H, dd, 14.2, 3.9) 4.39 (1H, dd, 14.2, 8.9)	51.6	4.78 (1H, dd, 14.3, 2.9) 4.53 (1H, dd, 14.3, 9.7)	51.3	4.64 (1H, dd, 14.5, 2.4) 4.28 (1H, dd, 14.5, 9.9)	45.7	4.61 (1H, dd, 14.5, 2.6) 4.25 (1H, dd, 14.5, 2.6)	40.0	4.77 (1H, d, 12.0) 4.34 (1H, m)	45.4	4.80 (1H, d, 14.2) 4.42 (1H, dd, 14.2, 9.7)	46.9
2'	4.25 (1H, dd, 8.9, 3.9)	72.7	4.13 (1H, m)	71.9	4.50–4.59 (1H, m)	77.3	4.01–4.16 (1H, m)	74.0	4.32 (1H, m)	73.4	4.32 (1H, m)	73.6
3'		177.9	3.62–3.74 (2H, m)	58.6	3.81–3.96 (2H, m)	49.7	2.97–3.29 (2H, m)	55.2	3.77–3.85 (2H, m)	50.0	3.82–3.96 (2H, m)	50.4
1"									4.33 (1H, d, 7.8)	104.3	4.17 (1H, d, 7.6)	106.2
2"									3.28 (1H, t, 9.1)	77.3	3.21 (1H, t, 8.9)	77.2
3"									3.02 (1H, dd, 9.1, 9.3)	78.0	3.13 (1H, t, 8.9)	78.6
4"									3.37 (1H, t, 9.3)	75.5	3.44 (1H, t, 9.3)	75.2
5"									3.52 (1H, d, 9.7)	78.6	3.72 (1H, d, 9.8)	80.5
6"										172.3		173.2
1'"							2.88 (1H, dd, 13.9, 4.9) 2.78 (1H, dd, 13.9, 7.4)	37.4				
2'"							3.92 (1H, m)	58.1				
3'"								172.3				

DMD Fast Forward. Published on April 9, 2013 as DOI: 10.1124/dmd.113.051235
This article has not been copyedited and formatted. The final version may differ from this version.

Table 3. Kinetic parameters (mean ± SD) of ornidazole glucuronidation in HLMs, HKMs, UGT1A9 and UGT2B7 in the presence or absence of 2% BSA.

Glucurondation Kinetic Parameters		without BSA				with BSA			
		HLMs	HKMs	1A9	2B7	HLMs	HKMs	1A9	2B7
R-ornidazole	K_m (mM) [a]	20.1 ± 1.4	17.7 ± 4.0	15.6 ± 1.6	N.A.	3.9 ± 0.1	3.0 ± 1.2	12.4 ± 2.1	N.A.
	V_{max} (pmol/min/mg)	38.9 ± 1.1	33.1 ± 3.0	59.3 ± 4.7	N.A.	35.6 ± 0.4	39.7 ± 1.4	59.2 ± 7.9	N.A.
	K_{si} (mM) [a]	N.A.	N.A.	12.5 ± 1.3	N.A.	N.A.	N.A.	5.9 ± 1.0	N.A.
	CL_{int} (ml/min/kg)	1.9 ± 0.1	1.9 ± 0.3	3.8 ± 0.1	N.A.	9.3 ± 0.1	13.3 ± 0.8	4.8 ± 0.2	N.A.
	Goodness of fit (R^2)	0.9991 [b]	0.9896 [b]	0.9996 [c]	N.A.	0.9998 [b]	0.9957 [b]	0.9989 [c]	N.A.
S-ornidazole	K_m (mM) [a]	6.6 ± 1.3	3.2 ± 0.4	N.A.	3.8 ± 0.9	0.6 ± 0.1	0.6 ± 0.1	N.A.	1.2 ± 0.2
	V_{max} (pmol/min/mg)	54.1 ± 6.1	39.8 ± 1.3	N.A.	48.7 ± 7.1	56.8 ± 2.6	48.4 ± 1.4	N.A.	41.9 ± 3.5
	K_{si} (mM) [a]	30.2 ± 3.2	N.A.	N.A.	14.9 ± 3.6	36.2 ± 7.0	N.A.	N.A.	14.8 ± 2.5
	CL_{int} (ml/min/kg)	8.2 ± 0.8	12.3 ± 1.1	N.A.	12.7 ± 1.4	99.4 ± 9.5	71.3 ± 7.8	N.A.	36.2 ± 3.8
	Goodness of fit (R^2)	0.9969 [c]	0.9953 [b]	N.A.	0.9923 [c]	0.9944 [c]	0.9933 [b]	N.A.	0.9925 [c]

N.A., not applicable.

[a] Expressed as unbound ornidazole.

[b] Data were fit into the Michaelis-Menten model.

[c] Data were fit into the substrate inhibition model.

Figure 1

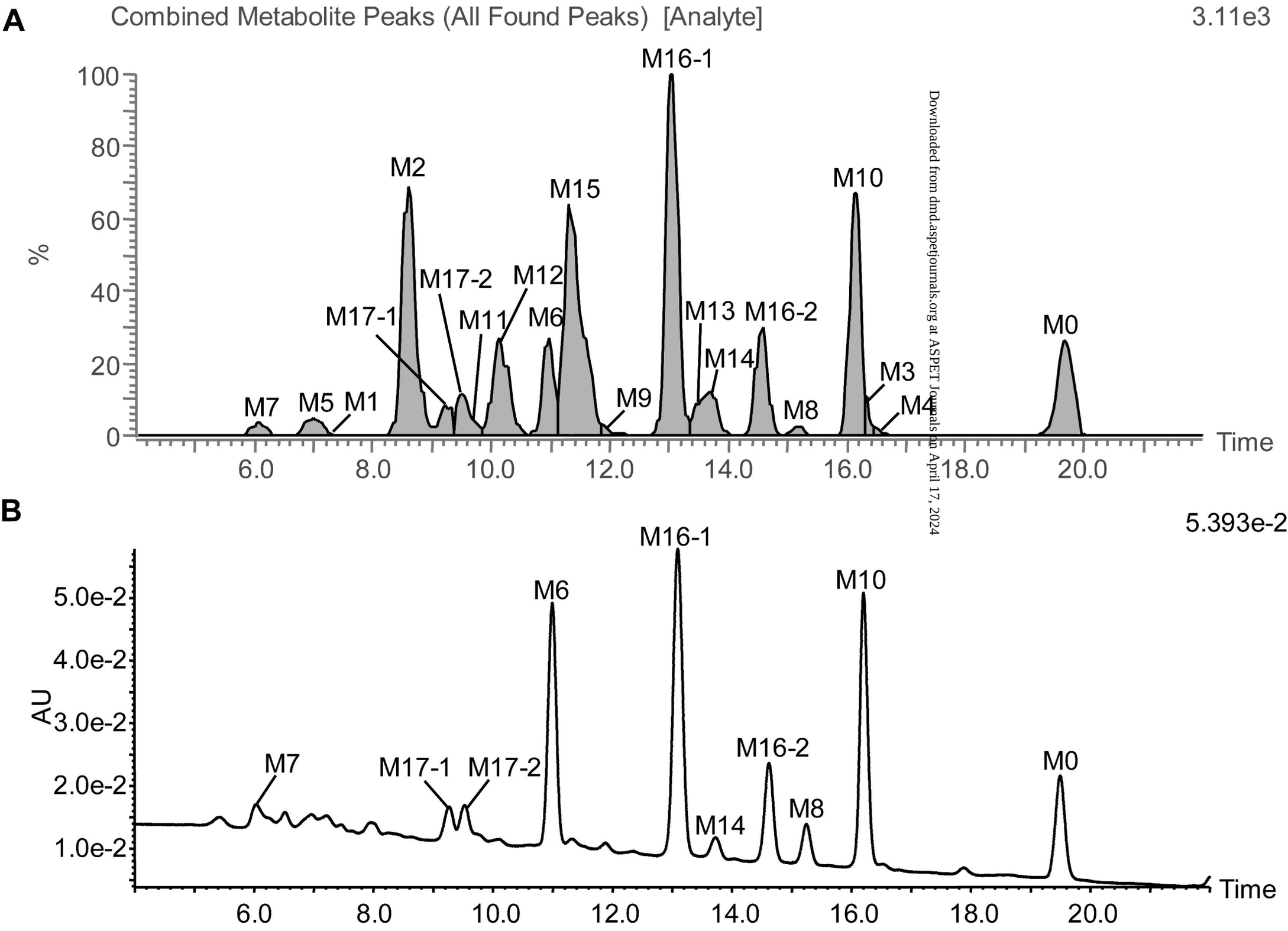
A
Combined Metabolite Peaks (All Found Peaks) [Analyte]
3.11e3
100
80
60
40
20
0
%
M16-1
M2
M15
M10
M17-2
M12
M17-1
M11
M6
M13
M16-2
M0
M14
M3
M7
M5
M1
M9
M8
M4
Time
6.0
8.0
10.0
12.0
14.0
16.0
18.0
20.0
Downloaded from dmd.aspetjournals.org at ASPET Journals on April 17, 2024
B
5.393e-2
5.0e-2
4.0e-2
3.0e-2
2.0e-2
1.0e-2
AU
M16-1
M6
M10
M7
M17-1
M17-2
M16-2
M0
M14
M8
Time
6.0
8.0
10.0
12.0
14.0
16.0
18.0
20.0

Figure 2

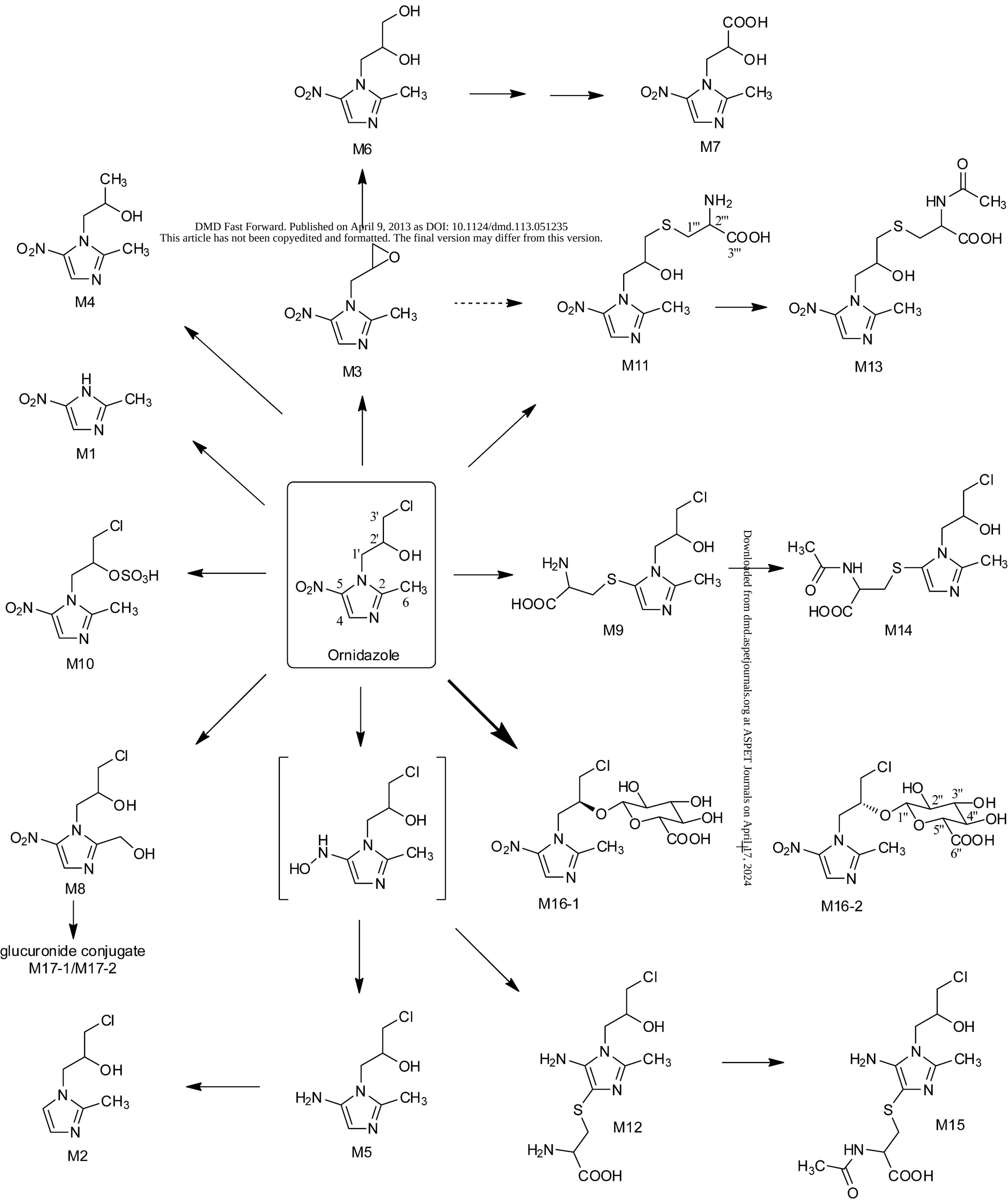

Figure 3

DMD Fast Forward. Published on April 9, 2013 as DOI: 10.1124/dmd.113.051235
This article has not been copyedited and formatted. The final version may differ from this version.

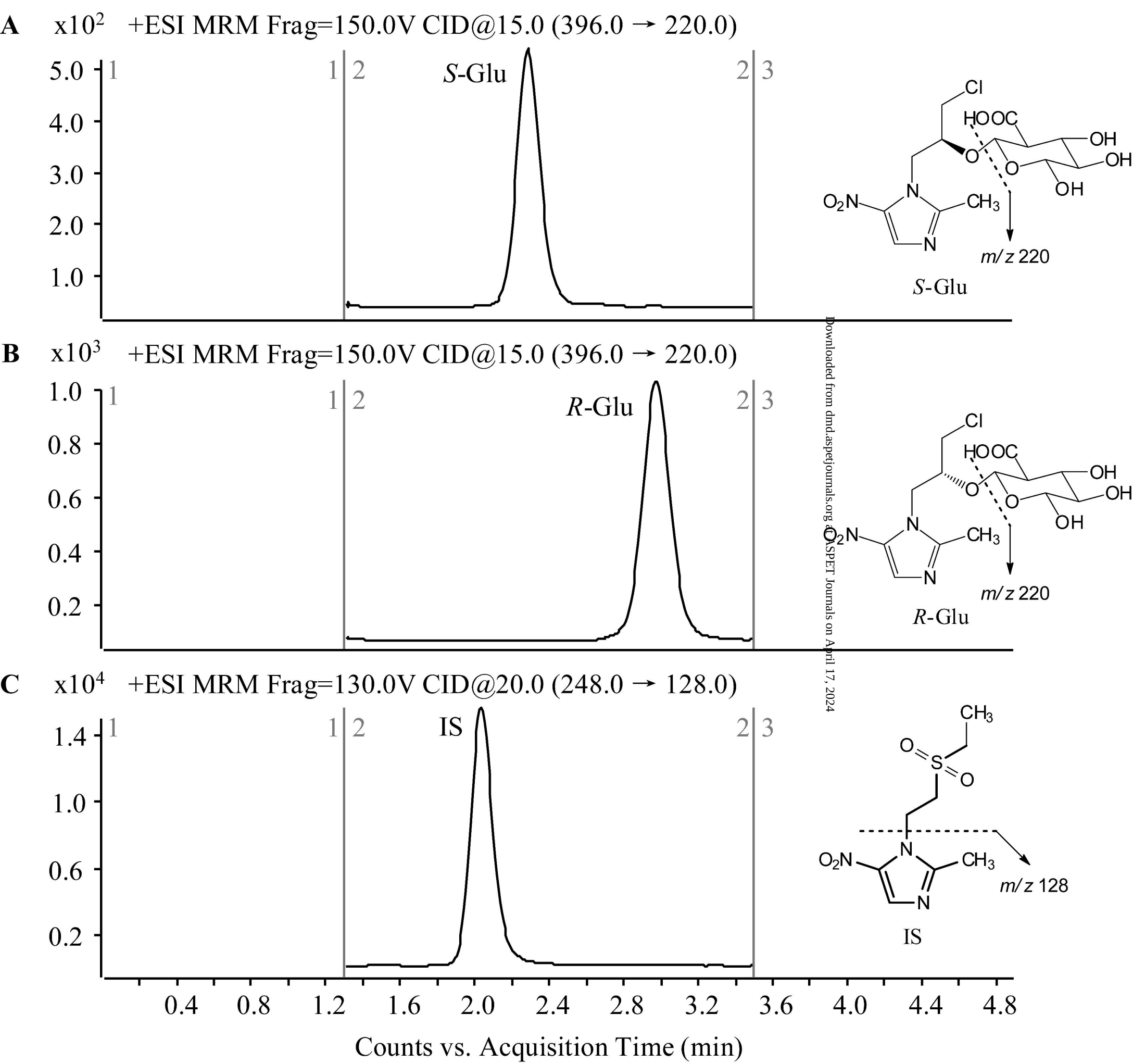

Figure 4

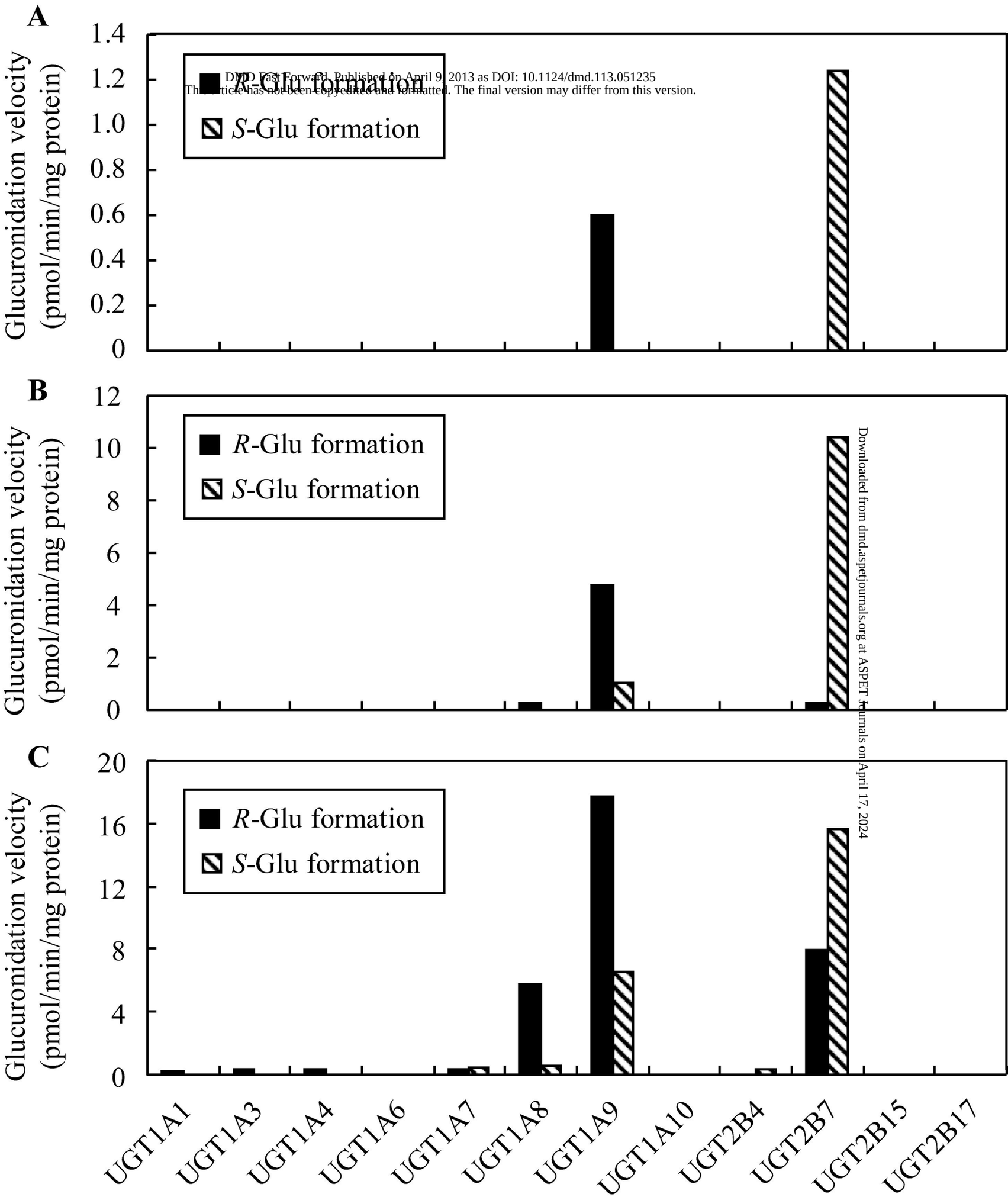

Figure 5

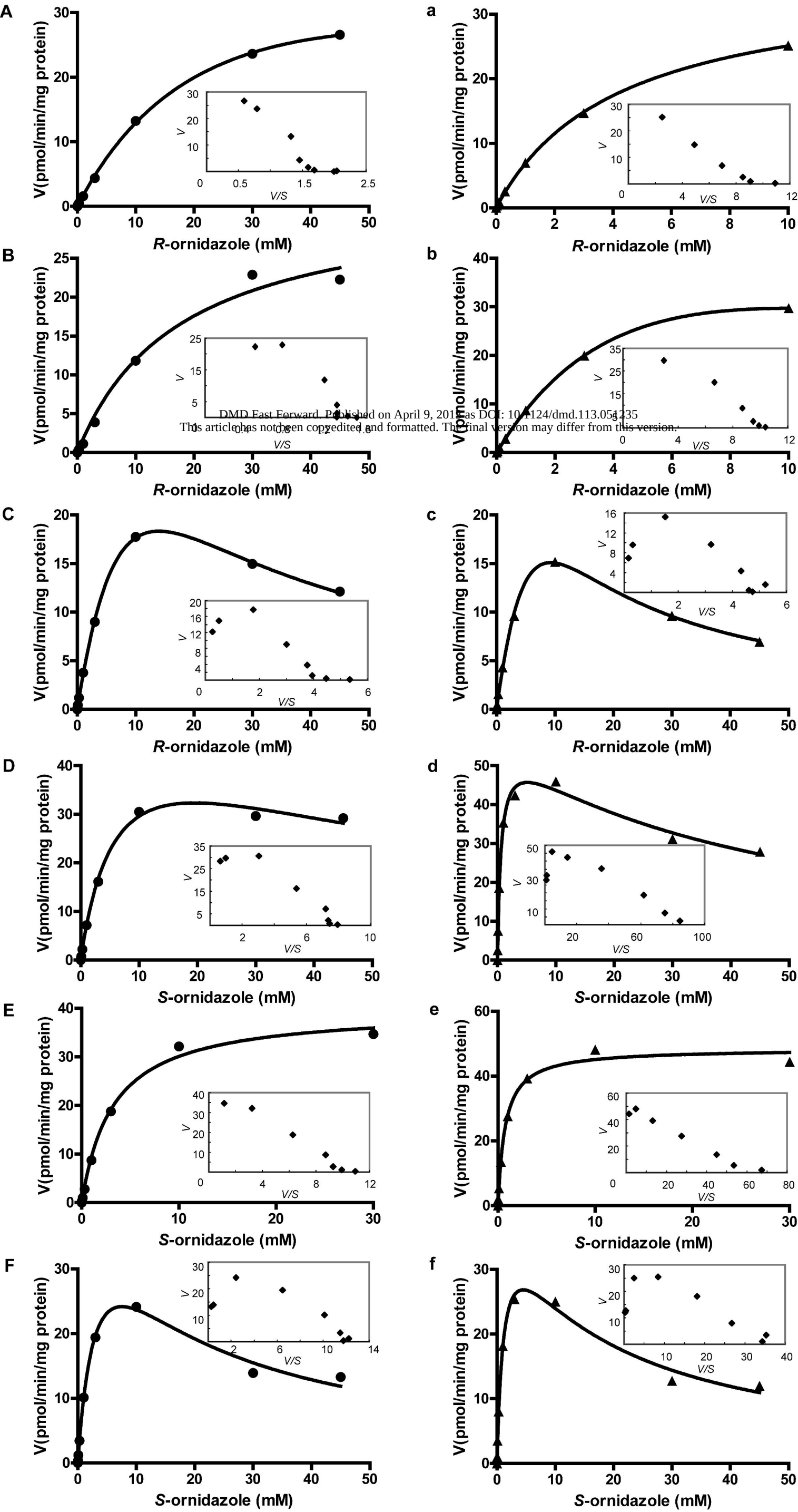

Figure 6

DMD Fast Forward. Published on April 9, 2013 as DOI: 10.1124/dmd.113.051235
This article has not been copyedited and formatted. The final version may differ from this version.